

MN-Pair Contrastive Damage Representation and Clustering for Prognostic Explanation

Takato Yasuno¹, Masahiro Okano¹ and Junichiro Fujii¹

¹Yachiyo Engineering, Co.,Ltd. Research Institute for Infrastructure Paradigm Shift, Japan.
{tk-yasuno, ms-okano, jn-fujii}@yachiyo-eng.co.jp

Abstract – It is essential for infrastructure managers to maintain a high standard to ensure user satisfaction during daily operations. Surveillance cameras and drone inspections have enabled progress toward automating the inspection of damaged features and assessing the health condition of the deterioration. When we prepare a pair of raw images and damage class labels, we can train supervised learning toward the predefined damage grade, displacement. However, such a damage representation does not constantly match the predefined classes of damage grade, hence, there may be some detailed clusters from the unseen damage space or more complex clusters from overlapped space between two damage grades. The damage representation has fundamentally complex features, consequently, all the damage classes could not be perfectly predefined. Our proposed MN-pair contrastive learning method enables us to explore the embedding damage representation beyond the predefined classes including more detailed clusters. It maximizes the similarity of M-1 positive images close to the anchor, and simultaneously maximize the dissimilarity of N-1 negative ones, using both weighting loss functions. It has been learning faster than the N-pair algorithm, instead of using one positive image. We propose a pipeline to learn damage representation and use density-based clustering on the 2-D reduction space to automate finer cluster discrimination. We also visualize the explanation of the damage feature using Grad-CAM for MN-pair damage metric learning. We demonstrate our method in three experimental studies: steel product defect, concrete crack of deck and pavement, and sewer pipe defect and mention its effectiveness and discuss potential future works.

Keywords –

Damage Representation; Density-Based Spatial Clustering; Damage Importance Explanation.

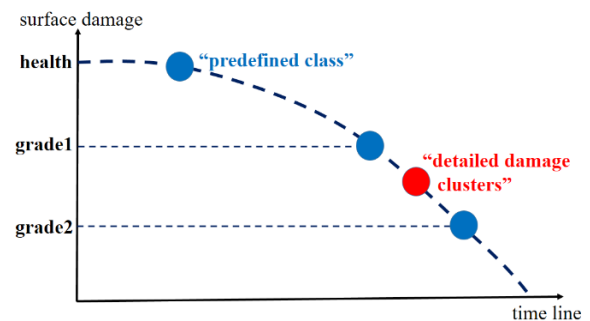


Figure 1. Predefined classes and finer clusters for prognostic damage understanding

1 Introduction

1.1 Objective and Pipeline

1.1.1 Contrastive Damage Metric Learning

Deep metric learning has been extensively investigated utilizing shared-parameter networks, such as Siamese and triplet networks [1]. Since 2013, various contrastive loss function minimizations for representation learning from similar/dissimilar pairs have been proposed [2]. For face recognition, verification, and clustering, several deep convolutional networks have been presented mapping from face images to a compact Euclidean space where distances correspond to a measure of face similarity [3][4]. Thus far, the usefulness of deep metric learning was not been sufficiently understood for recognizing our target of damaged surface similarity on infrastructures in the construction domain.

During a lifecycle of a deterioration process, the damaged surface of infrastructures frequently exhibits complex representations. When inspecting a surface for parts of structures using vision-based technology, qualitative grading classes are predefined to recognize damage, thereby recording the inspection. Despite potential unseen circumstances and ambiguous statuses between pre-defined classes, further experience may be necessary. Furthermore, complex defects may include

multi-damage, and mixing defect rather than anticipated in real-world structural monitoring.

Measuring the similarity of damage in high-dimensional vision images necessitates learning an embedding to a lower-dimensional damaged space. Once such a damage embedding space has been produced, vision-based inspection tasks such as damage recognition, diagnosis, and prognostic clustering can be easily implemented as standard techniques with damage embedding as feature vectors.

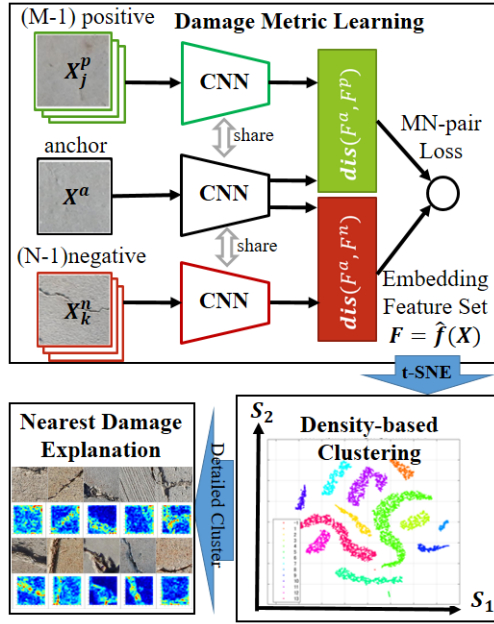


Figure 2. Our pipeline for damage representation learning, embedded clustering, and explanation

1.1.2 Damage Representation Clustering Pipeline

As shown in Figure 2, we propose a damage representation pipeline for learning damage features and clustering more detailed heterogeneous damages. The first training stage is developing a damage metric learning. Our proposed MN-pair contrastive learning method seeks to maximize the similarity of M-1 positive images to the anchor while simultaneously maximizing the dissimilarity of N-1 negative images, utilizing a weighting MN-pair loss function. Here, the triplet networks share the parameters under a convolutional neural network (CNN). The outputs of the damage embedding feature set with 16 elements are reduced to two dimensions using the t-SNE algorithm. The second clustering stage is density-based clustering toward more detailed damage clusters with the outlier option using the density-based spatial clustering application with noise (DBSCAN) algorithm. The third explanation stage is sorting the nearest feature scores and visualizing the tile of the nearest ten images. Furthermore, each image

enables us to compute heat maps using an adapted Grad-CAM algorithm for MN-pair damage metric learning.

2 Damage Representation Learning

2.1 MN-pair Damage Contrastive Learning

Let \mathbf{x} denote a set of inspected input images with predefined deterioration classes. Let $\mathbf{e}_i = f(\mathbf{x}_i; \boldsymbol{\theta}) \in R^L$ be the i -th damage embedding of input $i \in \{1, \dots, n\}$ that preserves the damage semantic aspects. Here, n is the number of input images. Furthermore, $\boldsymbol{\theta}$ is shared parameters under a CNN for damage metric learning, and L is the dimension of damage embedding space. Let $\mathbf{F}_i = \mathbf{e}_i / \|\mathbf{e}_i\|_2$ be the l_2 -normalized version. We can measure the damage similarity using the distance between two images i_1 and i_2 using the normalized cosine similarity,

$$s_{\theta}(\mathbf{x}_{i_1}, \mathbf{x}_{i_2}) = (\mathbf{F}_{i_1})^T \mathbf{F}_{i_2} \quad (1)$$

where larger values means more similarity. Here, the suffix T denotes transposed operation.

The N-pair loss approach [5] creates a multiclass classification in which we create a set of N-1 negative $\{\mathbf{x}_k^-\}_{k=1}^{N-1}$ and one positive \mathbf{x}_j^+ for every anchor image \mathbf{x}_i . We define the following N-pair loss for each set :

$$L_{N\text{-pair}}(\boldsymbol{\theta}; \mathbf{x}_i, \mathbf{x}_j^+, \{\mathbf{x}_k^-\}_{k=1}^{N-1}) = \log \left(1 - \exp(s_{\theta}(\mathbf{x}_i, \mathbf{x}_j^+)) + \sum_{k=1}^{N-1} \exp(s_{\theta}(\mathbf{x}_i, \mathbf{x}_k^-)) \right) \quad (2)$$

For simple expression, we denote cosine similarities as:

$$s_{i,j}^{a,+} = s_{\theta}(\mathbf{x}_i, \mathbf{x}_j^+) / \tau, \quad s_{i,k}^{a,-} = s_{\theta}(\mathbf{x}_i, \mathbf{x}_k^-) / \tau \quad (3)$$

Here, this is divided by a normalized temperature scale τ . This scale enhances small values, to ensure that N-pair loss is able to train efficiently, e.g. we can set the scale $\tau=0.3$. Thus, N-pair loss (2) is expressed as follows:

$$= -\log \frac{\exp(s_{i,j}^{a,+})}{\exp(s_{i,j}^{a,+}) + \sum_{k=1}^{N-1} \exp(s_{i,k}^{a,-})} \quad (4)$$

Note that the N-pair loss is the same as the InfoNCE loss [6][7]. However, the N-pair loss is a slow starter, because of only one positive image toward N-1 negative images. The positive signal is important for bonding the inner embedding space around the same class as every anchor.

Thus, we propose an MN-pair weighting loss instead of (2)(4), in which we create a set of N-1 negative $\{\mathbf{x}_k^-\}_{k=1}^{N-1}$ and M-1 positive $\{\mathbf{x}_j^+\}_{j=1}^{M-1}$ for every anchor \mathbf{x}_i :

$$L_{MN\text{-pair}}(\boldsymbol{\theta}; \mathbf{x}_i, \{\mathbf{x}_j^+\}_{j=1}^{M-1}, \{\mathbf{x}_k^-\}_{k=1}^{N-1}) = -\log \frac{v \sum_{j=1}^{M-1} \exp(s_{i,j}^{a,+})}{v \sum_{j=1}^{M-1} \exp(s_{i,j}^{a,+}) + w \sum_{k=1}^{N-1} \exp(s_{i,k}^{a,-})} \quad (5)$$

where v is a positive weight, and w is the negative weight constrained that $v + w = 1$, for example, $v = 0.15$. To train the parameters θ under a CNN for damage metric learning, we can minimize the MN-pair loss function $L_{MN-pair}$ using a standard optimizer, for example, the Adam.

2.2 Density-Based Damage Clustering

Using the damage-embedded feature F_i , $i \in \{1, \dots, n\}$ with the dimension L , we can reduce its dimension into two axes of scores using the t-SNE algorithm [8]. Several different notions exist of a cluster for damage representation for example, 1) well-separated clusters, 2) center-based clusters within a specified radius, and 3) density-based clusters. Under a two-dimensional damage embedding space, we can use either a center-based approach or a density-based one. The former is based on the distance from neighbor points to the center such as the K-means [9], and k-nearest neighbor [10]. To provide an effective approach to representing a heterogeneous subdivided region of damage beyond the predefined classes, we use the density-based clustering algorithm, i.e., the DBSCAN [11]. The points of embedding damage features are classified into 1) *core points* in the interior of a dense region, 2) *border points* on the edge of a dense region, and 3) *noise points* in a sparsely occupied region (a noise or background). The DBSCAN algorithm is formally given as follows:

1. Label all points as core, border, or noise points.
2. Eliminate noise points.
3. Put an edge between all core points that are within a user-specified distance parameter ϵ of each other.
4. Make each group of connected core points into a separate cluster.
5. Assign each border point to one of the clusters of its associated core points.

As we use a density-based definition of a cluster, it is relatively resistant to noise and can handle clusters of arbitrary damaged shapes. Therefore, DBSCAN can determine numerous damage clusters that could not be found using the center-based algorithm, for example, K-means. For damage representation clustering, we can set a distance parameter (for example, $\epsilon=3$) and a minimum number of neighbors for core points (for example, 10).

2.3 Nearest Damage Explanation

CNN models with millions of shared parameters achieve satisfactory performance for contrastive deep metric learning. Despite the impressive performance, the reasons for it remain unclear. This visualization technique is mainly divided into a masked sampling and an activation map approaches. The former includes the occlusion sensitivity [12] and the local interpretable model-agnostic explanations (LIME) [13]. The merits of

this approach do not require in-depth knowledge of the network's architecture, but the disadvantage is that it requires iterative computations per image, and running time for local partitioning, masked sampling, and output prediction. To represent damage metric contrastively, this output is not an image-based prediction output, but embedding damage feature F_i , $i \in \{1, \dots, n\}$ from a CNN output layer for contrastive damage metric learning. Therefore, we select an activation map approach such as the class activation map (CAM) [14] and gradient-based extension (Grad-CAM) [15]. The weighting feature map of the CAM is ineffective as it limits the global average pooling (GAP) and fully-connected (FC) at the concluding layer of a CNN.

Inspired by the work of [16], we propose a gradient-based visualization technique for damage metric learning. The final layer of our proposed MN-pair contrastive learning is a damage feature embedding space FC with the size of $1 \times 1 \times L$. Unlike a classification model, we could not specify any pair of similarity between anchor, positive, and negative because of numerous combinations of their pairs. Practically we propose a *reduced similarity score* as a *reduction function* to enhance an average powered similarity for damage explanation as follows:

$$y^S(\mathbf{U}) = \sum_{m=1}^K (U^m)^2 \quad (6)$$

where $\mathbf{U} = (U^1, \dots, U^K)$ is an embedding damage feature with K dimensions before the final output layer with the size of $1 \times 1 \times K$ as a *reduction layer*, for example, FC $1 \times 1 \times 128$. To obtain the similarity contrastive localization map $G_{Grad-CAM}^S \in R^{W \times H}$, we can compute the gradient of the reduced similarity score $y^S(\mathbf{U})$ with respect to feature map activations $A^m(x, y)$ of convolutional or ReLU as a *feature layer*, i.e., $\partial y^S / \partial A^m$. Here, A^m has the size of array $W \times H \times K$, for example, ReLU $20 \times 20 \times 128$. These gradients flowing back are global averages pooled over the width x and height y , respectively to obtain the similarity importance weights.

$$\alpha_m^S = \frac{1}{WH} \sum_x \sum_y \frac{\partial y^S}{\partial A^m(x, y)}, m = 1, \dots, K. \quad (7)$$

Thus, this weight α_m^S represents partial linearization of the CNN downstream from feature map activations A^m , and captures the similarity importance. We can perform a weighted combination of forward activation maps for damage similarity representation learning.

$$G_{Grad-CAM}^S = ReLU \left(\sum_{m=1}^K \alpha_m^S A^m \right). \quad (8)$$

3 Applied Results

We demonstrated experimental studies using our method and applied it to three datasets of damage.

3.1 Damage Dataset and Training Setup

We implemented experiments using open-accessed datasets of steel product defect (11,638 samples from Steel Defect Detection [17]), concrete crack on deck and pavement (12,633 samples from SDNET2018 [18]), and sewer pipe defect (19,690 samples from Sewer-ML [19][20]). Table 1 illustrates each dataset for experimental studies that contains target damage, the number of predefined classes, and the partition of training and test images, respectively.

Table 1. Datasets for experimental studies

Target damage	Predefined Classes	Number of training/test
Steel product defect	5	8,148 / 3,490
Concrete crack	4	8,844 / 3,789
Deck, pavement		
Sewer pipe defect	4	13,134 / 6,556

Table 2. Summarized the size of input damage images and the number of clusters from the results of density-based DBSCAN clustering under the damage embedding space with two dimensions reduced by the t-SNE. Surprisingly, our contrastive damage representation learning provided two or more multiplied clusters toward the number of predefined classes in Table 1.

Table 2. Training image size and clustering results

Target damage	Input Image Size [h,w]	Density-Based Output of Clusters
Steel product defect	[256, 256]	10
Concrete crack	[256, 256]	13
Deck, pavement		
Sewer pipe defect	[576, 768]	17

As listed in Table 3, we set the layer type and output shape of the CNN architecture under our experimental studies. We set a simple but practical network with 15 layers that contain convolution-ReLU-max pooling and FC. This architecture has neither batch normalization nor skip connection. We set the mini-batch to 128 and the number of iterations to 2,000–5,000 while training the CNN network to obtain a stable loss curve. We used the Adam optimizer with a learning rate of 0.0001, and set the gradient decay factor to 0.9, and the squared gradient decay factor to 0.99. We used image augmentation using random erasing [21][22]. We set the input size to 160×160×3, after conducting ablation studies on 128, 144, 160, 180, and 200. We also set the output dimension

of damage embedding space to 16 practically, after conducting ablation studies on 8, 16, and 32. Furthermore, we set the temperature scale to 0.3 practically, compared with ablation studies with 0.1, 0.2, 0.3, and 0.5. Finally, we set the hyperparameters of MN-pair damage contrastive learning $M=N$ to 4 and 5, as the number of classes on the target dataset. We also set the positive weight to $v = 0.15$ practically, compared with ablation studies with 0.1, 0.15, 0.2, and 0.3. For written space restriction, we have to cut these ablation studies, where the evaluation index is the overall accuracy from damage feature-based classification trained to test the dataset. For computing the gradient-based activation map Grad-CAM, we set the feature layer to Relu4 and set the reduction layer to FC1 in Table 3.

Table 3. Layer type and shape of CNN architecture

Layer type	Output Shape (S,S,C)	Params #
Conv1-Relu1	160,160,8	224
Maxpool1	80,80,8	--
Conv2-Relu2	80,80,32	2,336
Maxpool2	40,40,32	--
Conv3-Relu3	40,40,64	18,496
Maxpool3	20,20,64	--
Conv4-Relu4	20,20,128	73,856
FC1-Relu5	1,1,128	6,553,728
FC2	1,1,16	2,064
total	Learables	6.6M

3.2 Steel Defect Representation Results

3.2.1 Steel Defect Embedding Clustering

Figure 3 illustrates the result of steel defect clustering using five colors under damaged embedding space by the t-SNE. The predefined 1st normal class (red), 3rd inclusion (light green), and patch defect (magenta) have been subdivided into two or three regions.

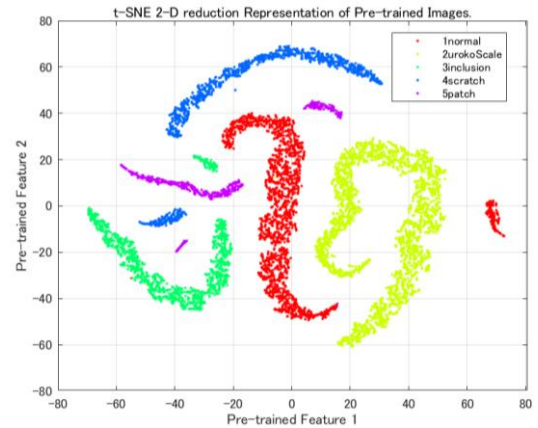


Figure 3. Trained five classes of steel product defect 2-D reduced outputs via t-SNE

Figure 4 provided the results of density-based 11 clusters using eleven HSV-based colors from 1 to 11. Note that there is an outlier from a predefined 4th scratch class.

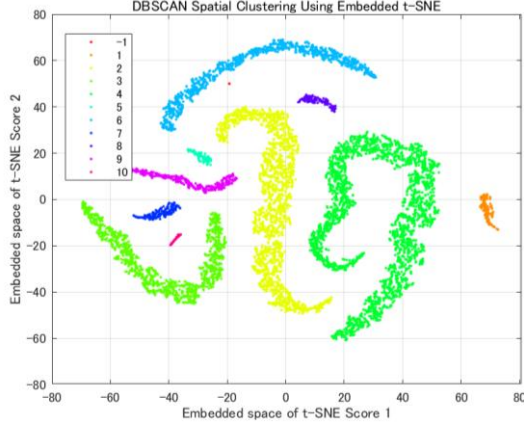


Figure 4. Steel product defect of density-based clustered into ten using DBSCAN

3.2.2 Steel Defect of Each Cluster Nearest Images

Figure 5 depicts the density-based ten steel clusters in each row of images where the first column one is sampled and the right nine images with the nearest similarity score.

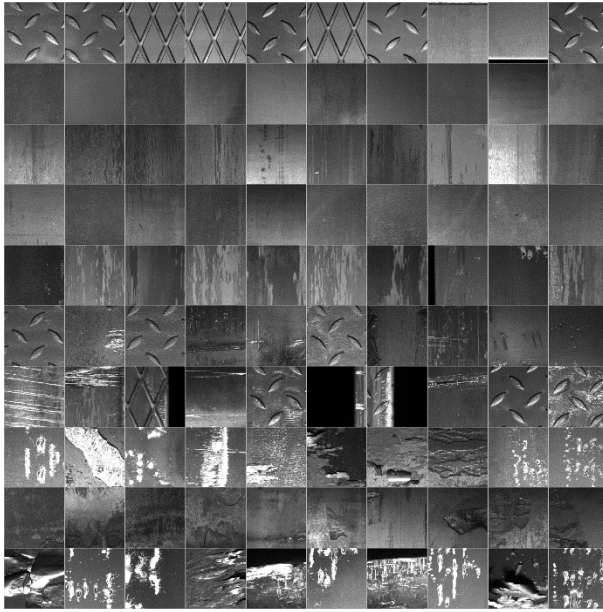


Figure 5. Density-based ten clusters in each row of images, the first column is sampled, and right nine nearest images

3.2.3 Steel Product Defect Explanation

Figure 6 illustrates the result of steel defect explanation computing gradient-based activation map using Grad-CAM for contrastive damage metric learning. The order of rows and columns is the same as in Figure

5. These heat maps explain the damage feature of steel defect clusters.

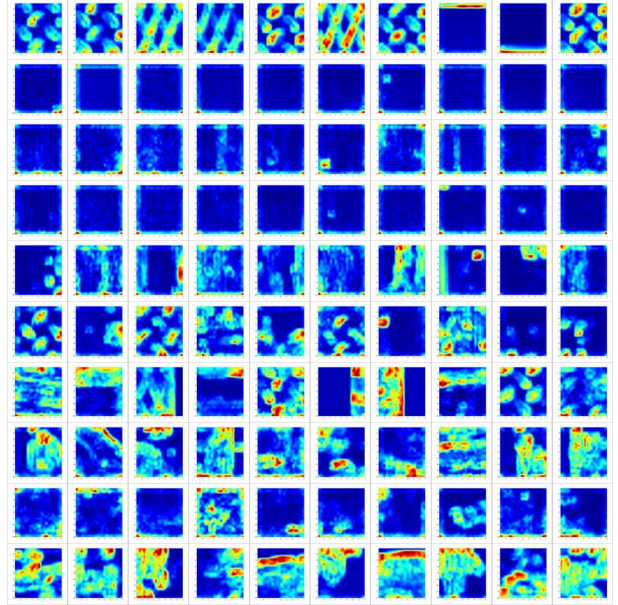


Figure 6. Steel defect of damage explanation

3.3 Concrete Crack Representation Results

3.3.1 Concrete Crack Embedding Clustering

Figure 7 illustrates the result of crack clustering using four colors under damaged embedding space by the t-SNE. The predefined 1st deck-crack class (red), 3rd pavement-crack (light green), and pavement-non-crack (magenta) have been subdivided into three or four regions.

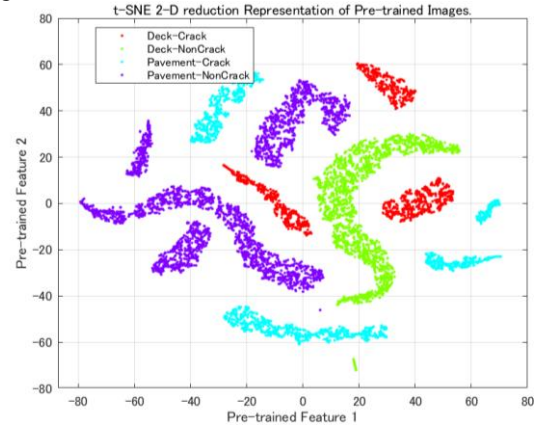


Figure 7. Trained four classes of concrete damage 2-D reduced outputs via t-SNE

Figure 8 provides the results of density-based 14 clusters using eleven HSV-based colors numbering from 1 to 14. Note that one outlier exists in the fourth class of non-crack pavements.

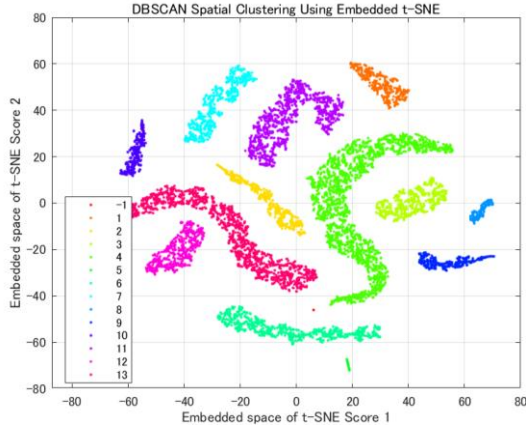


Figure 8. Concrete damage of density-based clustered into 13 using DBSCAN

3.3.2 Concrete Crack Clusters Nearest Images

Figure 9 shows the 13 density-based crack clusters in each row image, with the first column sampled and the nine images to its right having the nearest similarity score. The deck and the pavement subgroup were divided.



Figure 9. Thirteen density-based clusters in each row of images, the first column is sampled, and right nine images with nearest similarity scores

3.3.3 Concrete Crack Explanation

Figure 10 illustrates the result of crack explanation computing gradient-based activation map using Grad-

CAM for contrastive crack metric learning. The arrangement of rows and columns is consistent with that in Figure 9. These heat maps explain the damage feature of crack clusters, and also discriminate each background texture between the deck surface and pavement surface.

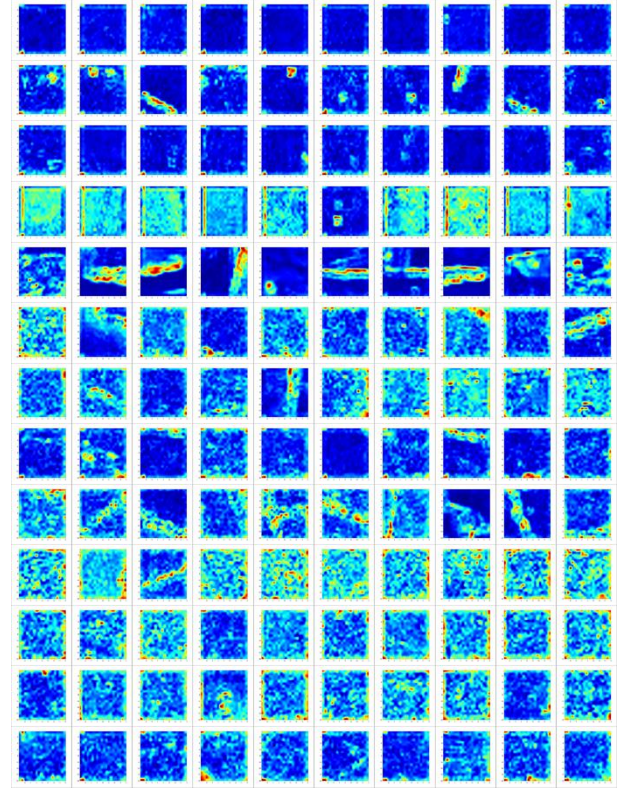


Figure 10. Concrete crack of damage explanation

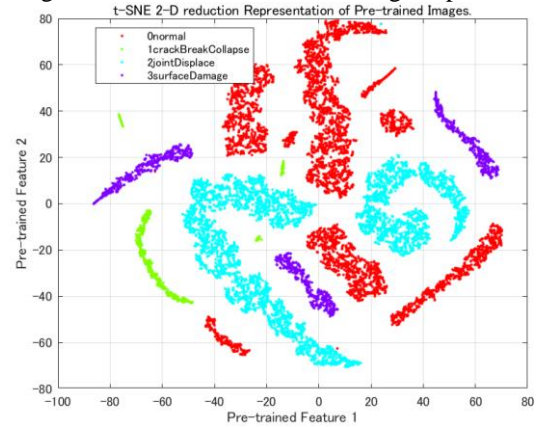


Figure 11. Trained 4 classes of sewer pipe defect 2-D reduced outputs via t-SNE

3.4 Sewer Pipe Defect Representation Results

3.4.1 Sewer Pipe Defect Embedding Clustering

Figure 11 illustrates the result of sewer pipe defect clustering using four colors under damaged embedding space by the t-SNE. Surprisingly, the predefined 1st

normal class (red) has been subdivided into eight regions, because of various pipe locations. The predefined 2nd crack-break-collapse (light green) has been subdivided into four regions that contain extremely small regions, because of the rare event with less variation. The 3rd joint displacement (sky blue) was divided into two regions. Finally, the predefined 4th surface damage has been subdivided into three regions. The density-based 17 clusters using seventeen HSV-based colors numbered 1 to 17 yielded the results displayed in Figure 12, with no outliers present.

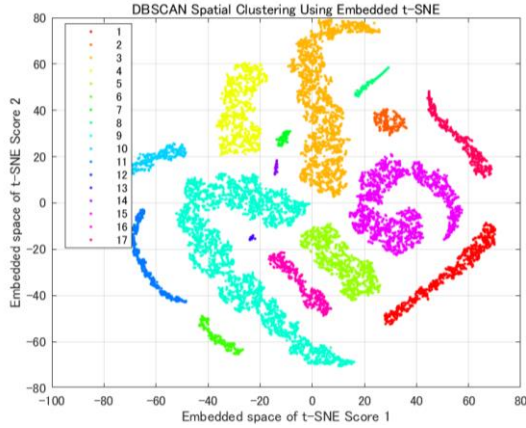


Figure 12. Sewer pipe defect of density-based clustered into 17 using DBSCAN

3.4.2 Sewer Pipe Defect Cluster Nearest Images

Figure 13 shows 17 density-based clusters of sewer pipe defects in each row of images, with the first column being sampled and the other nine being the nearest score. The background location was almost divided.

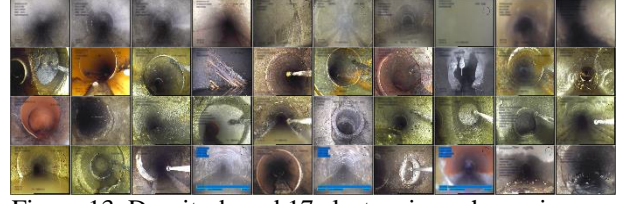


Figure 13. Density-based 17 clusters in each row images where the first column is sampled and the right 9 images with nearest similarity score

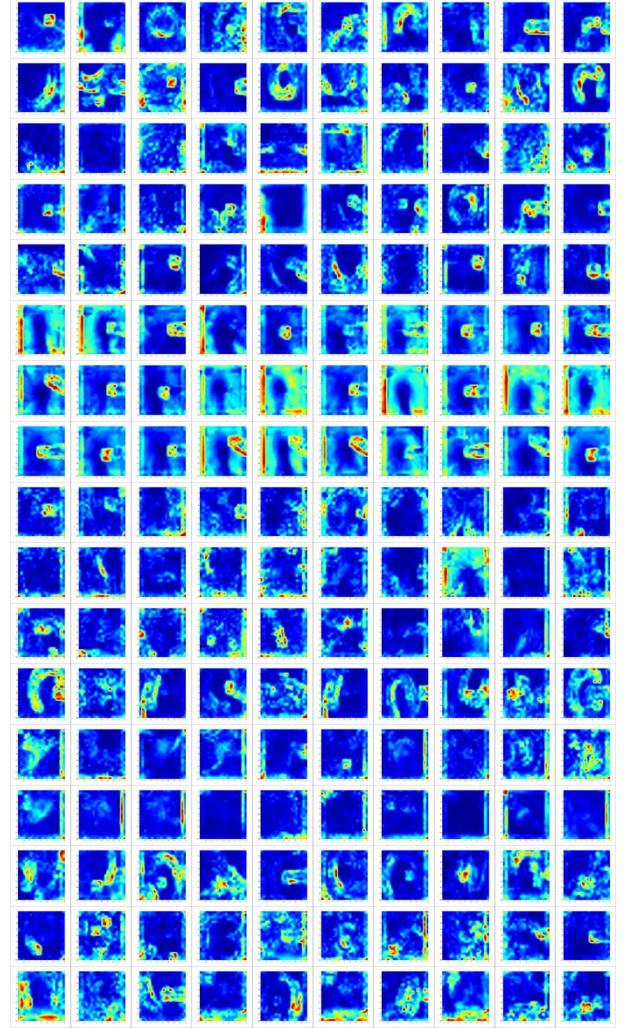


Figure 14. Sewer defect of damage explanation

3.4.3 Sewer Pipe Defect Explanation

Figure 14 illustrates the result of sewer pipe defect explanation computing gradient-based activation map using Grad-CAM for contrastive sewer defect learning. The order of rows and columns is the same as in Figure 13. This heat map elucidates the more complex and ambiguous damage features of sewer pipe defect clusters. These maps discriminate each background texture between different locations over the sewer pipe area.

4 Concluding Remarks

4.1 Experimental Results

We proposed a contrastive learning and clustering pipeline for damage representation. Practically, we have formulated the MN-pair damage embedding space for the anchor, M-1 positive images, and also N-1 negative ones. The shared network architecture was a simple but practical convolutional network with 15 layers. Furthermore, we propose a clustering method using the output of an MN-pair damage embedding space after two dimensional-reduction by the t-SNE and the density-based DBSCAN clustering. Furthermore, the authors present the gradient-based damage explanation to adapt for the final activation map from the convolutional network trained by an MN-pair contrastive damage representation learning.

We found that the Damage feature exhibited considerable heterogeneous variation, rather than the pre-defined classes determined by human inspection. The damaged embedding space had an unexpected increase in the number of detailed clusters. We demonstrated our method in three experimental studies using the open accessed datasets, such as steel product of surface defects, concrete cracks of decks and pavements, and sewer pipe defects. We confirmed the efficacy of the proposed method for surface damage datasets.

4.2 Future Works

There are more practical problems for *co-defect* representation where one image has a multi-label and bordered region between damaged pair of classes. A hard negative sampling scheme would be contributed. For *robustness* of heterogeneous damage, mixture and erasing augmentation would improve performance. For *faster* computation, MLP-based network would be an option. For *applicability*, other trials could be water quality, disaster scene, and LCZ built-up/natural classes.

Acknowledgment We thank Takuji Fukumoto (Math-Works Japan) who supports the MATLAB resources.

References

- [1] Kaya, M. Bilge, H.S. Deep Metric Learning: A Survey, *Symmetry*, MDPI, 2019.
- [2] R. Karsten, Milbich T. et al. Revisiting Training Strategies and Generalization Performance in Deep Metric Learning, *Proceedings of 37th International Conference on Machine Learning, PMLR*, 2020.
- [3] Schroff, F. Kalenichenko, D. FaceNet: A Unified Embedding for Face Recognition and Clustering, *arXiv:1503.03832v3*.
- [4] Chopra, S. Hadsell, R. Learning a Similarity Metric Discriminatively with Application to Face Verification, *CVPR* 2005.
- [5] Sohn K. Improved Deep Metric Learning with Multi-class N-pair Loss Objective, *30th Conference on Neural Information Processing Systems*, 2016.
- [6] Khosla, P. Teterwak P. et al. Supervised Contrastive Learning, *34th Conference on Neural Information Processing Systems, NeurIPS*, 2020.
- [7] Oord, A. Li, Y. and Vinyals, O. Representation Learning with Contrastive Predictive Coding, *arXiv:1807.03748v2*.
- [8] Linderman, G.C., Steinerberger, S. Clustering with t-SNE, Provably, *Society for Industrial and Applied Mathematics*, Vol.1, No.2, pp313-332, 2019.
- [9] Hartigan J. A. et al. K-Means Clustering Algorithm, *Journal of the Royal Statistical Society. Series C*, Vol. 28, No. 1, pp. 100-108, 1979.
- [10] Comak, E., Arslan, A. A New Training Method for Support Vector Machines: Clustering k-NN SVM, *Expert Systems with Applications* 35, pp564–568, 2008.
- [11] Evangelos, S. Jiawei, H. et al. A Density-Based Algorithm for Discovering Clusters in Large Spatial Databases with Noise, *Proceedings of the Second International Conference on Knowledge Discovery and Data Mining (KDD-96)*, 1996.
- [12] Zeiler, M.D. et al. Visualizing and Understanding Convolutional Networks, *arXiv:1311.2901v3*.
- [13] Ribeiro, M.T., S. Sameer Why Should I Trust You? Explaining the Predictions of Any Classifier, *Knowledge Discovery and Data Mining, KDD* 2016.
- [14] Zhou, B., Khosla, A., Lapedriza A. et al. Learning Deep Features for Discriminative Localization, *arXiv:1512.04150v1*.
- [15] Selvaraju, R.R., Cogswell M. et al. Grad-CAM: Visual Explanations from Deep Networks via Gradient-based Localization, *ICCV*, 2017.
- [16] Zhu, S., Yang T. et al., Visual Explanation for Deep Metric Learning, *arXiv:1909.12977v4*.
- [17] <https://github.com/zdaioi/Kaggle-Steel-Defect-Detection>, Accessed 17/6/2021.
- [18] Dorafshan, S., Thomas, R.J. et al. SDNET2018: An Annotated Image Dataset For Noncontact Concrete Crack, <https://doi.org/10.1016/j.dib.2018.11.015>, Accessed 15/12/2022.
- [19] Haurum, J.B., Moeslund T.B. et al. Sewer-ML: A Multi-Label Sewer Defect Classification Dataset and Benchmark, *IEEE Xplore, CVPR2021*.
- [20] Sewer-ML defect dataset, <https://vap.aau.dk/sewer-ml/>, Accessed 15/12/2022.
- [21] C. Shorten, T.M. Khoshgoftaar A Survey on Image Data Augmentation for Deep Learning”, *Journal of Big Data*, 6:60, 2019.
- [22] Zhongyx, Z. Zheng, L. et al. Random Erasing Data Augmentation, *arXiv:1708.04896v2*.